Biogeosciences
Open Access
Discussions

Landscape-scale changes in forest structure and functional traits along an Andes-to-Amazon elevation gradient

G. P. Asner[1], C. Anderson[1], R. E. Martin[1], D. E. Knapp[1], R. Tupayachi[1],
T. Kennedy-Bowdoin[1], F. Sinca[1], and Y. Malhi[2]

[1]Department of Global Ecology, Carnegie Institution for Science, 260 Panama Street, Stanford CA 94305, USA
[2]School of Environment and Geography, University of Oxford, South Parks Road, Oxford OX1 3QY, UK

Correspondence to: G. P. Asner (gpa@carnegiescience.edu)

Discussion Paper | Discussion Paper | Discussion Paper | Discussion Paper

Abstract

Elevation gradients provide opportunities to explore environmental controls on forest structure and functioning, but plot-based studies have proven highly variable due to limited geographic scope. We used airborne imaging spectroscopy and LiDAR (light detection and ranging) to quantify changes in three-dimensional forest structure and canopy functional traits in a series of 25 ha landscapes distributed along a 3300 m elevation gradient from lowland Amazonia to treeline in the Peruvian Andes. Canopy greenness, photosynthetic fractional cover and exposed non-photosynthetic vegetation varied as much across lowland forests (100–200 m) as they did from the lowlands to the Andean treeline (3400 m). Elevation was positively correlated with canopy gap density and understory vegetation cover, and negatively related to canopy height and vertical profile. Increases in gap density were tightly linked to increases in understory plant cover, and larger gaps (20–200 m^2) produced 25–30 times the response in understory cover than did smaller gaps (< 5 m^2). Scaling of gap size to gap frequency was, however, relatively constant along the elevation gradient, which when combined with other canopy structural information, indicates equilibrium turnover patterns from the lowlands to treeline. Our results provide a first landscape-scale quantification of forest structure and canopy functional traits with changing elevation, thereby improving our understanding of disturbance, demography and ecosystem processes in the Andes-to-Amazon corridor.

1 Introduction

Tropical elevation gradients offer natural laboratories for studies of environmental controls on forest composition, structural habitats, functional processes, and ecosystem development (Vitousek et al., 1992). To date, most studies have employed field-based observations to quantify elevation-related changes in nutrient cycling, productivity and a variety of plant traits (e.g., Alves et al., 2010). Results from such studies have shown

that species composition often changes markedly with increasing elevation in the tropics (Silman, 2006; Lieberman et al., 1996), yet patterns of canopy functional traits and productivity have proven much more variable (e.g., Vitousek et al., 1988; Raich et al., 1997; Girardin et al., 2010). Indeed field-based elevation studies report wide-ranging results that have proven challenging to synthesize into generalizable patterns and emergent principles (Tanner et al., 1998; Hodkinson, 2005).

While reports on elevation-based changes in functional processes vary widely in the tropics, patterns of forest structural traits such as volume, canopy layering and gap dynamics remain even less understood. Yet structure expresses the outcome of, and mediates the future of, functional processes such as light use, canopy turnover and NPP (Asner et al., 1998; Brokaw, 1985b). Structure also creates the habitat for all other forest-dwelling species (Terborgh, 1992), so developing a quantitative understanding of forest structural change with elevation is requisite to conservation and management planning.

A significant and persisting problem limiting our understanding of elevational patterns in forest functional and structural properties rests in accessing remote field sites and the canopies that occupy those sites. In most cases, sub-montane to montane forests have proven the most difficult to study, owing to rough terrain, poor road and river access, and arduous overland distances. Another problem centers on ecological scale; nearly every study thus far published on elevation-related changes in tropical forest properties has focused either on individual species or in plots no larger than a hectare. Yet habitats can change very quickly at a given elevation, simply based on slope, aspect and disturbance. This challenges efforts to determine average effects of elevation on canopy structural properties and functional processes.

Remote sensing offers a means to address these challenges by providing observations and measurements of forests at larger geographic scales. However, persistent cloud cover common to tropical elevation gradients has limited the utility of satellite-based observations (Ticehurst et al., 2004). Airborne platforms offer a solution because the measurements can be planned around local cloud cover dynamics. From the air,

Landscape-scale changes in forest structure

G. P. Asner et al.

Title Page

Abstract | Introduction

Conclusions | References

Tables | Figures

|◄ | ►|

◄ | ►

Back | Close

Full Screen / Esc

Printer-friendly Version

Interactive Discussion

remote measurement of canopy functional and structural properties has become increasingly common. Forest functional traits, including light interception, foliar cover and canopy chemistry, are often reported using spectral data collected with imaging spectrometers (Kokaly et al., 2009; Ustin et al., 2004). Forest canopy structure is increasingly being explored using airborne Light Detection and Ranging (LiDAR) systems (Lefsky et al., 2002; Drake et al., 2002). Combined, imaging spectroscopy and LiDAR represent a uniquely powerful approach, providing demonstrably high data dimensionality, for probing the composition, structure and functioning of ecosystems (Asner et al., 2012b). However, these newer technologies have rarely, if ever, been applied to tropical elevation gradients.

The Andes-to-Amazon corridor stretches 2000 km from Colombia to Bolivia, and from elevations of ~ 100 m in the Amazon lowlands to nearly 4000 m at the Andean treeline. The forest canopy is comprised of thousands of plant species arranged in communities associated with changing elevation, geology, soils and hydrological conditions (Gentry, 1988). To date, most studies of forest functional and structural patterns have focused on the Amazon lowlands, demonstrating that forest canopy height, aboveground biomass and foliar nutrient concentrations vary by community, soil type and geologic substrate (Quesada et al., 2009; Baker et al., 2004; Fyllas et al., 2009). A recent study found that canopy gap-size frequency distributions – a quantitative expression of turnover patterns – are surprisingly constant throughout the southwestern Amazonian lowlands (Asner et al., 2013a).

In comparison to the lowlands, we have little knowledge of canopy structural and functional variation on elevation gradients up to Andean treeline. Recent 1 ha plot studies on an Andes-Amazon elevation gradient suggest that aboveground biomass decreases with increasing altitude (Girardin et al., 2010). However, the landscape-scale biomass patterns remain unknown, and are likely to vary widely based on the pronounced floristic, topographic, geologic, and soil variability found throughout the region (INGEMMET, 2000; Hoorn et al., 2010). Plot studies also indicate that biomass turnover rates do not systematically change with increasing elevation, despite declines

in plot-level biomass stocks from the lowlands to treeline (Girardin et al., 2013). In addition, leaf area index (LAI) and photosynthetic capacity (A_{max}) remain nearly constant along the elevation gradient (Y. Malhi, unpub. data), corresponding to consistently high concentrations of leaf nitrogen (Asner et al., 2013b). However, both NPP and GPP do decline at higher elevations, above 1500 m a.s.l., and this is associated with increased cloud cover and decreased irradiance at higher elevations (Girardin et al., 2010; Huaraca Huasco et al., 2013). If plot-scale biomass and productivity indeed decline at higher elevations, how does biomass turnover remain fairly constant? The answer likely rests in relative changes in canopy gap formation and regrowth, neither of which has been nor likely could be measured at landscape scales on the ground.

To address these unknowns, we quantified landscape-scale changes in forest canopy structural and functional properties from lowland Amazonia to the Andean treeline in Peru. Our assessment was carried out at an ecological scale thus far unachieved in the field – 25 ha forest landscapes in 20 unique abiotic settings described by varying elevation, climate and soils. We used the Carnegie Airborne Observatory (CAO) Airborne Taxonomic Mapping System (AToMS) to collect multi-dimensional measurements of vegetation (Asner et al., 2012b), and to answer these questions about Western Amazonian ecosystems: (i) How does local terrain below the forest canopy change with elevation? (ii) How do canopy height and the vertical partitioning of the vegetation change with elevation? (iii) Do canopy gaps co-vary with changes in canopy structure along an elevation gradient? (iv) How do canopy functional traits such as light interception, photosynthetic and non-photosynthetic vegetation cover, and greenness change with elevation? (v) Do structural and functional traits co-vary with one another, and if so, how does elevation affect relationships between traits? (vi) Do remotely sensed canopy functional and structural traits support and extend plot-based suggestions of nearly constant biomass turnover despite decreasing biomass stocks along an Andes-to-Amazon elevation gradient?

2 Methods

2.1 Study landscapes

Twenty study landscapes, each of 25 ha in size, were selected for mapping across northern, central and southern Peru (Table 1), centered mainly around 1 ha plots that have been the focus of forest inventories (Peacock et al., 2007), and/or intensive carbon budget analysis (Malhi et al., 2010). In these landscapes, mean annual precipitation ranges from 1705 to 5020 mm yr^{-1}. Mean annual temperature varies from 12.5 °C at the highest elevation sites in the Andes to 26.6 °C in the warmest lowland site. Soils in the lowland landscapes vary among three broad classes: Ultisols on *terra firme* clay substrates, Inceptisols on inactive high-fertility floodplains of late Holocene age, and Entisols in two locales in northern Peru. These Entisols are the well-known white sand substrates associated with very low nutrient availability (Fine et al., 2004). In the Andean landscapes, soils are classified as Inceptisols or well-developed Entisols (Quesada et al., 2009).

2.2 Airborne data collection

The airborne data were collected in August–September 2011. CAO AToMS includes a Visible-to-shortwave Infrared (VSWIR) imaging spectrometer and a dual laser, waveform LiDAR (Asner et al., 2012b). These sub-systems are hardware and digitally boresight aligned onboard a Dornier 228–202 aircraft. We collected AToMS data over each study landscape from an altitude of 2000 m a.g.l. at an average flight speed of 55–60 m s^{-1} and a mapping swath of 1200 m.

The VSWIR spectrometer collects data in 481 contiguous spectral channels spanning the 252–2648 nm wavelength range with 5 nm (full-width at half-maximum) bandwidth. It has a 34°, field-of-view and an instantaneous field-of-view of 1 mrad. At 2000 m a.g.l., the VSWIR data collection provided 2 m ground sampling distance, or pixel size, throughout each study landscape. The LiDAR has a beam divergence set to 0.5 mrad,

Landscape-scale changes in forest structure

G. P. Asner et al.

Title Page

Abstract | Introduction

Conclusions | References

Tables | Figures

◀ | ▶

◀ | ▶

Back | Close

Full Screen / Esc

Printer-friendly Version

Interactive Discussion

and was operated at 200 kHz with 17° scan half-angle from nadir, providing swath coverage similar to the VSWIR spectrometer. Because the CAO AToMS data were collected from adjacent flightlines with 50 % overlap, the LiDAR point density achieved was 2 shots m^{-2}, or 8 shots per VSWIR pixel.

2.3 Data processing

Laser ranges from the LiDAR were combined with the embedded high resolution Global Positioning System-Inertial Measurement Unit (GPS-IMU) data to determine the 3-D locations of laser returns, producing a "cloud" of LiDAR data. The LiDAR data cloud consists of a very large number of georeferenced point elevation estimates (cm), where elevation is relative to a reference ellipsoid (WGS 1984). To estimate canopy height above ground, LiDAR data points were processed to identify which laser pulses penetrated the canopy volume and reached the ground surface. We used these points to interpolate a raster digital terrain model (DTM) for the ground surface. This was achieved using a 10 m ×10 m kernel passed over each flight block; the lowest elevation estimate in each kernel was assumed to be ground. Subsequent points were evaluated by fitting a horizontal plane to each of the ground seed points. If the closest unclassified point was < 5.5° and < 1.5 m higher in elevation, it was classified as ground. This process was repeated until all points within the block were evaluated. The digital surface model (DSM) was based on interpolations of all first-return points. Measurement of the vertical difference between the DTM and DSM yielded a model of canopy height above ground (digital canopy model, DCM).

The vertical distribution of LiDAR points was processed by binning the data into volumetric pixels (voxels) at 5 × 5 m spatial and 1 m vertical resolution (Asner et al., 2008). The DTM was used to standardize the vertical datum of each voxel. Therefore, the heights of each vertical "slice" of a vegetation canopy were defined relative to the ground at the horizontal center of each voxel. After all LiDAR points were binned in the volume cube, each vertical column of the cube was divided by the total number of LiDAR points in that column, yielding the percentage of LiDAR points that occurred in

Full Screen / Esc

Printer-friendly Version

Interactive Discussion

each voxel. This approach has the advantage of decreasing our sensitivity to localized variations in canopy leaf density or tree branch characteristics, which can result in a different number of LiDAR returns from voxel to voxel.

The VSWIR data were radiometrically corrected from raw DN values to radiance (W sr^{-1} m^{-2}) using a flat-field correction, radiometric calibration coefficients and spectral calibration data collected in the laboratory. The standardized GPS pulse-per-second measurement was used to precisely co-locate VSWIR spectral imagery to the LiDAR data collection. We created a camera model to precisely describe the three-dimensional location and field-of-view of each sensor and, combined with standardized timing information, for high-precision data co-registration. A smoothed best estimate of trajectory (SBET), LiDAR DTM, and camera model were then used to produce an image geometry model and observational data containing information on exact solar and viewing geometry for each image pixel. These inputs were used to atmospherically correct the radiance imagery using the ACORN-5 model (Imspec LLC, Glendale, CA USA). To improve aerosol corrections in ACORN-5, we iteratively ran the model with different visibilities until the reflectance at 420 nm (which is relatively constant for vegetated pixels) was 1 %. Reflectance imagery was then corrected for cross-track brightness gradients using a bidirectional reflectance distribution function (BRDF) model described by Colgan et al. (2012). The imagery was then geo-orthorectified to the LIDAR DCM. In addition, the precise positioning of the LiDAR-to-VSWIR data allowed for automated masking of pixels shaded by neighboring canopies and branches, as well as water bodies (Fig. A1) (Asner et al., 2007).

2.4 Analysis

Descriptive statistics were generated from the LiDAR-derived DCM and DTM for each study landscape. In addition, topographic slope and aspect were computed using a 5 m ×5 m moving kernel on the DTM. The vertical canopy profile data were averaged, plotted and compared among landscapes. From the vertical canopy profile maps, we analyzed elevation-dependent variation in understory (below upper canopy) vegetation

cover in 1–3 m, 3–5 m, and 5–10 m slices above ground level. In addition, we computed a canopy shape parameter for each landscape – the ratio of the height above ground where maximum canopy volume occurs (P) to the 99th percentile of total canopy height (H). The $P : H$ ratio reduces a large amount of LiDAR vertical profile information into a simple metric depicting the overall architecture of the canopy. A high $P : H$ ratio indicates that the majority of foliage is positioned high in the canopy; a low $P : H$ ratio indicates a groundward tendency of foliar distribution.

We mapped and analyzed gaps in the forest canopy by applying a definition similar to Brokaw's (1982) definition to the DCM results whereby all gaps down to 2 m above ground level were mapped and their areas quantified. We also quantified the gap-size frequency distribution using the Zeta distribution, which is a discrete power-law probability density as described in detail by Asner et al. (2013a). For the Zeta distribution with parameter λ, the probability that gap size takes the integer value k is:

$$f(k) = \frac{k^{-\lambda}}{\zeta(\lambda)} \tag{1}$$

where the denominator is the Riemann zeta function, and is undefined for $\lambda = 1$. This distribution is sometimes called the "discrete Pareto distribution", and is appropriate for modeling the size-frequency of canopy gaps (Clauset et al., 2007; Fisher et al., 2008; White et al., 2008).

CAO VSWIR spectrometer images were used to generate a series of remotely sensed metrics of canopy functional traits. The results were compared at the landscape level following the application of a water and shade mask (Fig. A1), which was derived from the co-aligned LiDAR data. The normalized difference vegetation index (NDVI) was calculated as (NIR-VIS)/(NIR+VIS), where NIR and VIS were reflectances at 800 and 680 nm, respectively. The fraction of intercepted photosynthetically active radiation (fIPAR) was mapped by subtracting the canopy reflectance in the 400–700 nm PAR range, band by band from 100 % reflectance, and then taking the mean of the difference among PAR spectral bands (Wessman et al., 1998).

We mapped the fractional lateral cover of photosynthetic vegetation (PV), non-photosynthetic vegetation (NPV), and bare substrate (S) surfaces in each 2 m VSWIR pixel using the AutoMCU algorithm (Asner and Heidebrecht, 2002). The AutoMCU is a linear spectral mixture model that incorporates spectral endmember libraries for PV, NPV and S derived from multiple data sources described by Asner (2008). Briefly, the PV spectral library was derived from airborne imaging spectrometer measurements of tropical canopy trees; NPV and S were derived from field spectrometer measurements across a wide range of tropical forest non-photosynthetic materials and soils. Critically, the PV and NPV fractional cover outputs isolate the lateral percentage cover of exposed live and dead/senescent tissues; this is not equivalent to LAI or other volume-integrating properties of canopy foliage content (Asner et al., 2005).

3 Results

3.1 Terrain

LiDAR DTMs indicated eleven landscapes with mean elevations $\leq$ 223.3 m a.s.l., four from 496.2–1712.9 m a.s.l., and five from 1831.5–3379.3 m a.s.l. (Table 2). Hereafter for convenience, we refer to these three groups as lowland, sub-montane and montane landscapes. Among the lowland landscapes, the variance in elevation was very low, with a maximum-recorded standard deviation (SD) of just 6.7 m on the ALP-30 landscape (Fig. 1). Coefficients of variation (CV) in elevation averaged 1.1 % among lowland landscapes. Slope on a 5×5 m kernel basis ranged from a mean (+ SD) of 2.4° (2.2°) to 9.7° (5.2°). Throughout the lowlands, topographic aspect was oriented mostly in the North-South direction ($\sim$ 154–192° true N).

In the sub-montane zone, we found that two landscapes – PJL-01 at 496.2 m and PJL-02 at 884.1 m – straddled a transition in topographic relief along the elevation gradient (Fig. 1). PJL-01 contained relief more similar to the other lowland landscapes, with a narrow elevation SD = 5.6 m, shallow slopes (6.7° ± 5.6°, and North-South ori-

Full Screen / Esc

Printer-friendly Version

Interactive Discussion

ented aspects (182.3° ± 111.3° (Table 2). In contrast, PJL-02 harbored much greater elevational variation with a CV = 7 % compared to 1 % at PJL-01. Topographic slope increased to 31.8° ± 9.6° at PJL-02, and aspect shifted to 143.5° ± 80.8°. This transition marked a fundamental change in terrain in terms of relief, slope and aspect that persisted into the montane landscapes. Throughout the montane forests under study, mean topographic slope ranged from 28.6–41.8°. Mean aspect varied from 121.4° to 189.8°, with the exception of ESP-01 with a mean aspect of 246.4°.

3.2 Remotely measured canopy structure

Along the elevation gradient, forest canopy height decreased from 24.5 ± SD 7.3 m in the lowest lying landscape (SUC-01) to 8.9 ± 5.6 m in our highest landscape (TRU-01) (Fig. 2, Table 2). Note that we masked out the river in TAM-06 in all of our vegetation analyses (Fig. A1). Elevation accounted for 72 % of the regional variation in mean canopy height ($p < 0.001$; RMSE = 2.75 m). This occurred despite the fact that two lowland landscapes on dystrophic white sands (JEN-12, ALP-40) harbored vegetation with locally suppressed canopy height (15.1–16.5 m).

As we crossed the terrain transition from PJL-01 and PJL-02, the canopy opened up with increased prevalence of landslides at PJL-02 as well as in landscapes SPD-01 and SPD-02 further upslope (Fig. 2). Coefficients of variation in canopy height increased from an average of 33.7 % for all lowland landscapes, to 43.4 % for these three sites harboring increased landslide activity. At the highest elevations, the landscapes contained a sparse array of tall (> 25 m) trees embedded in a matrix of shorter-statured (3–6 m) vegetation. This resulted in high variance of canopy height while halving of the mean canopy height (Table 2).

We measured the canopy gaps reaching 2 m above ground level on a per-hectare basis in each 25-ha landscape (Fig. 3a). The number of gaps ha^{-1} increased linearly with elevation ($p < 0.05$). For example, smaller gaps of < 5 m^2 size were 50 % more frequent in the montane than in the lowland landscapes. This was true for most other gap-size classes as well. In addition, independent of elevation, smaller gaps of < 5 m^2

were about ten times more common than gaps of 5–10 m^2, which in turn, were about ten times more common than gaps of 50–200 m^2. The gap-size frequency exponent λ varied in the lowlands from about 1.75 (large gaps) to 2.25 (small gaps) (Fig. 3b). However, we found a weak linear decrease in λ with elevation ($R^2 = 0.09$, $p<0.05$) among sub-montane and montane landscapes (dotted circles in Fig. 3b).

Using the vertical canopy profile data from the LiDAR, we discovered systematic changes in canopy architecture with increasing elevation as well as by lowland soil type (Fig. 4). In lowland landscapes, canopies often reached heights of 40–44 m, with the bulk of the canopy volume situated 20–25 m above ground level (Fig. 4a). We note that the TAM-09 landscape also contained a vegetation layer about 2–3 m above ground, associated with swamp and riparian vegetation found along the Tambopata River. In contrast, the lowland landscapes on the white sands (JEN-12, ALP-40) contained canopies reaching lower maximum heights of 32–37 m, and with leaves more evenly distributed throughout the vertical profile (Fig. 4b).

The canopy $P:H$ shape ratio was strongly and negatively correlated with elevation ($R^2 = 0.68$; $P<0.001$; RMSE $= 0.11$) (Table 2). $P:H$ was 0.56 ± 0.04 for lowland canopies on non-sand substrates. For sands, $P:H$ declined to 0.35 ± 0.08, indicating a ground-ward shift in the vertical distribution of foliage. Canopies in the four sub-montane sites contained trees that often exceeded 40 m in height, but the vertical partitioning of the foliage shifted ground-ward in comparison to the lowland, non-sand landscapes (Fig. 4c). $P:H$ for these sites was 0.50 ± 0.05 (Table 2). We also found a pronounced understory layer in the 1–5 m height range. Low-statured vegetation cover further increased in the montane landscapes, with nearly all vegetation dominating classes < 10 m in height (Fig. 4d). We note, however, that even the montane forests contained some trees approaching and exceeding 30 m in height. $P:H$ ratios for the montane landscapes were 0.12 ± 0.05, indicating a strong ground-ward shift in the vertical partitioning of the vegetation in the highest Andean Amazon forests.

We further investigated the vertical layering of the vegetation by mapping three discrete height classes or layers (1–3 m, 3–5 m, and 5–10 m) in each 25 ha landscape

(Fig. 5). Note that these maps do not simply present canopy height data; instead, they are maps of canopy cover within specific vertical strata either beneath the overstory canopy or as low-stature vegetation in gaps (Asner et al., 2012b). In the lowland landscapes, these maps revealed a spatial match between canopy gaps (Fig. 2) and vegetation in these short height classes. For example, the two white sand landscapes contained large patches of 1–3 m and 3–5 m tall vegetation (yellow colors, Fig. 5). Among the sub-montane landscapes, particularly the three with obvious signs of landslides, vegetation in the slide areas was 1–3 m in height (red colors, Fig. 5). Additional increases in elevation up to the montane sites resulted in large areas of each landscape dominated by lower-statured vegetation in the 1–10 m height classes. Our field observations indicate that this lower stature vegetation in montane landscapes is dominated by gap-colonizing *Chusquea* bamboos and ferns. Regression analyses of these three vertical canopy layers indicated consistent linear increases in the percentage of understory and low-statured vegetation cover with elevation (Fig. 6).

We also discovered consistent relationships between the number of gaps per hectare and the percentage cover of low-statured vegetation (Fig. 7). Specifically, we found monotonically increasing understory cover with increasing gaps ha^{-1}, but at different rates depending upon gap size classes of 0–5 m^2 to $\geq$ 200 m^2. The larger the gap class, the steeper the slope between understory vegetation cover and elevation. These patterns were consistent in the 1–3 m, 3–5 m, and 5–10 m understory vegetation height classes. Increases in the number of gaps ha^{-1} in the 0–5 m^2 gap-size classes resulted in the slowest increase in understory plant cover. The opposite was true for the largest ($\geq$ 200 m^2) gap class.

3.3 Remotely measured canopy function

With the CAO VSWIR spectrometer, we mapped canopy spectral characteristics throughout each 25 ha landscape. Sites ESP-01 and TRU-01 were not imaged due to poor atmospheric conditions during overflight (Fig. 8). Inspection of the color-infrared images, each of which is histogram-matched for comparison, indicated that lowland

sites contain a mix of canopies with high near-infrared (NIR) reflectance values shown in red, and lower values in blue. The two landscapes containing the highly dystrophic white sand soils (JEN-12, ALP-40) showed larger, semi-contiguous patches of suppressed NIR reflectance. Among three of the sub-montane landscapes, the presence of landslides was also obvious as blue linearly-shaped patches (Fig. 8). Otherwise, intact canopies in these sub-montane areas showed generally high NIR reflectances. The pattern changed substantially again in the montane landscapes, which show widespread decreases in NIR reflectance.

Plotting the VSWIR-derived canopy functional properties against elevation revealed two contrasting patterns (Fig. 9). First, among lowland landscapes, the site-level mean NDVI spanned a range of 0.87 to nearly 0.90 (Fig. 9a). Canopies on Entisols (white sands) and Inceptisols (floodplains) in the lowlands had a slightly suppressed average NDVI as compared to canopies on *terra firme* Ultisols. Second, the widely varying NDVI in the lowlands gave way to a systematic decrease in NDVI with increasing elevation among sub-montane and montane sites (adj-R^2 = 0.80; t = −4.97; p<0.005). This lowland versus sub-montane/montane NDVI pattern was repeated in the measurement of lateral fractional cover of photosynthetic vegetation (PV) among the landscapes (Fig. 9b). In fact, the range of PV in the lowlands exceeded the monotonic decrease among sub-montane to montane sites spanning nearly 3000 m of elevation gain. Both the lowland and upland PV patterns were mirrored by changes in non-photosynthetic vegetation (NPV) and bare soil fractions (Fig. 9c–d). NPV increased monotonically, while bare soil decreases with elevation.

These changes in NDVI, PV, NPV and bare soil fractions occurred despite a lack of elevation trend in the fraction of photosynthetically active radiation intercepted by the vegetation (fIPAR). In fact, fIPAR remained nearly constant and highly saturated at 0.98 (s.d. = 0.01) among sites, and there was no relationship with elevation (adj-R^2 = 0.17; p = 0.10).

3.4 Structural-functional relationships

We computed Pearson Product Moment correlations relating the measured canopy structural and functional traits (Table 3). Any relationships described here were significant at the $p \geq 0.05$ level. The NDVI was inversely correlated with the fractional cover of non-photosynthetic vegetation (NPV) and bare substrate (S), and positively correlated with structural properties including canopy height ($r = 0.83$) and shape ($P : H$; $r = 0.86$). NDVI was consistently negatively correlated with the number of gaps ha^{-1} in all gap-size classes except for the very largest gaps ($r = -0.58$ to -0.82), and therefore was also negatively correlated with percentage cover of vegetation 1–10 m above ground level. Although canopy fIPAR was high and nearly saturated throughout the elevation gradient, it was negatively correlated with the number of canopy gaps ha^{-1} as well as vegetation cover in the 1–5 m height classes.

Among the canopy structural properties, height was positively correlated with shape ($P : H$) and negatively associated with gaps ha^{-1} and low-statured vegetation in all size and height classes, respectively (Table 3). The gap-size frequency parameter λ was also negatively correlated with gaps ha^{-1} and vegetation in the 1–3 m height class. Finally, many of the gap-size classes were inter-correlated, while canopy height was not related to the gap size-frequency λ.

4 Discussion

Very few regions of the world offer 3200 m of elevation change while maintaining humid tropical forest conditions. The gradient considered in this study provided this rare setting to assess the role that elevation plays in determining vegetation structure, functional traits, and their interactions. Although elevation was the primary independent factor of interest here, we also found a relationship between elevation and slope (Pearson Product Moment $r = 0.78$; $p<0.05$). Moreover, we found that the terrain hidden beneath the forest canopy changed in non-systematic ways: (i) landscapes below 500 m

a.s.l. harbored mostly flat terrain; (ii) a transition occurred between 500 m and 880 m elevation from lowland to montane terrain conditions; and (iii) landscapes above 880 m to treeline bore steep terrain (Fig. 1). Higher elevations are usually associated with steeper slopes in tectonically active areas, consistent with coarser resolution data from across the region (e.g., Regard et al., 2009).

These threshold changes in topography were, to some extent, expressed in non-systematic changes in canopy functional traits. For example, we found very wide-ranging values of NDVI, PV, NPV and bare substrate throughout the lowlands, which then gave way to monotonic changes in these functional metrics above 400 m elevation (Fig. 9). Because NDVI, PV and NPV are well known correlates of canopy greenness, leaf cover, and exposed non-photosynthetic vegetation, respectively (Roberts et al., 1997; Asner et al., 2005; Gamon et al., 1995), we conclude here that the western Amazon lowlands harbor variation in canopy functional traits often exceeding that produced by 3200 m of elevation change to Andean treeline. This highlights the degree to which lowland canopies respond to regional patterns of geologic, hydrologic, and soil fertility variation (Tuomisto et al., 2003; Carvalho et al., 2013), also expressed in shifting community composition, productivity, and carbon storage (Quesada et al., 2009; Asner et al., 2012a; Higgins et al., 2012; Aragão et al., 2009; Girardin et al., 2013).

In contrast to the dominant pattern of functional variation in the lowlands, most canopy structural properties were very closely tied to changes in elevation alone. For example, the number of gaps ha^{-1} (Fig. 3) and the percentage cover of understory vegetation (Fig. 6) were consistent in the lowlands and then linearly increased to treeline. Canopy height and the canopy $P : H$ ratio also declined linearly with elevation (Table 2). Moreover, we discovered systematic changes in the vertical distribution of plant tissues in lowland to sub-montane, and to montane forest environments (Fig. 4). Exceptions to these rules were found in the two highly dystrophic, white sand landscapes in northern Peru (JEN-12, ALP-40), which harbored locally suppressed canopy height and a ground-ward shift in canopy vertical profiles. So while elevation is the regionally

Landscape-scale changes in forest structure

G. P. Asner et al.

dominant control on canopy structural characteristics, soil fertility also plays a role in creating structural diversity among a subset of lowland forest types (Fig. 10).

Although we discovered a number of elevation-dependent trends in canopy characteristics, we also found coordinated variation among many of the properties. For example, canopy height and shape were highly correlated, and both of these properties were negatively related to gap density (Table 3). Moreover, (Fig. 3), while canopy height decreased with elevation (Table 2). In Peruvian forests, canopy height (CH) is highly correlated with aboveground biomass ($0.4356*CH^{1.7551}$; $R^2 = 0.89$; $p < 0.001$), whereas stand-level wood density is not ($R^2 = 0.08$; $p = 0.16$) (Asner et al., 2012c). Therefore, canopy height is an excellent surrogate for aboveground biomass along our elevation gradient. Our 25 ha landscape scale decreases in aboveground biomass greatly extend the 1 ha plot-scale estimates of the same (Girardin et al., 2010, 2013).

Since aboveground biomass decreases with elevation, concurrent with increases in canopy gap density, then biomass turnover must be relatively constant when ascending from the lowlands into the montane. This finding is well supported by our near-constant gap-size scaling parameter λ (Fig. 3), which is a quantitative index often used to compare and contrast biomass turnover rates in tropical forests (Gloor et al., 2009; Asner et al., 2013a; Chambers et al., 2013). If any trend does exist for λ, it suggests a slight decrease with increasing elevation indicative of larger gaps, likely related to landslides. Recently, Malhi et al. (unpub. data) found that biomass turnover is fairly constant with increasing elevation in 1 ha plots spread across the elevation gradient. Not only does our work corroborate these plot-based studies, it suggests that we can use airborne remote sensing of gap-size frequency and canopy height to infer relative rates of turnover over millions of hectares of forests from lowland to treeline. Doing so will improve our understanding of the spatial distribution of growth and mortality at much larger ecological scales than can be achieved in plot studies.

Given that biomass turnover remains relatively constant with elevation, what causes the steep decline in the NDVI with increasing elevation (Fig. 9a)? Traditionally, NDVI has been associated with light interception, leaf area index (LAI), and canopy nitro-

gen content, among other parameters (Hatfield, 1984; Goward and Huemmrich, 1992; Sellers et al., 1995; Myneni et al., 1997). However, we found that fractional intercepted PAR, or fIPAR, was saturated and nearly constant among the twenty 25 ha landscapes throughout our elevation and soils gradient, so there is very little chance that the NDVI is related to light interception or LAI. By definition, this decouples the NDVI from gross and net primary production in the direct light-absorption sense of the relationship (Nemani and Running, 1989). Instead, we found the NDVI to be negatively correlated with gap density (Table 3), but not with the fractional cover of photosynthetic vegetation (PV). This suggests that the NDVI might be inappropriate for use in modeling primary production in Amazonian forests, especially within the sub-montane to montane reaches of the Andes. Instead, the NDVI is more sensitive to turnover, which as we described, appears to be an indirect proxy for production at steady state. The precise connection between changing NDVI and gap density likely rests in increased greenness associated with regrowing vegetation in large canopy gaps (Riano et al., 2002), which are found in increasing density with elevation on our gradient.

Our results provide insight into the relationship between disturbance and understory plant cover. Understory cover increases with elevation (Fig. 10). This trend is driven by increases in gap density, but at differential rates depending upon gap size and vegetation height (Fig. 7). It takes about 25–30 times the number of 0–5 m^2 gaps to produce understory responses created in a single 20–200 m^2 gap. These results suggest a strong limiting role of low light availability on understory plant cover in forests spanning the lowland Amazon to the Andean treeline. Although this issue is already well appreciated in the tropical forest literature (Denslow, 1987; Lawton, 1990), quantification of light response thresholds have remained elusive due to the impracticalities of field measurements in highly heterogeneous understory light environments (Chazdon, 1988). Here we show that, for western Amazonian forests, gaps larger $\gg 5$ m^2 result in the largest understory plant cover increases. Yet independent of gap size or density, the percentage cover of understory plants never exceeds 8 % per hectare for 1–3 m or 3–5 m tall plants, while it often reaches but does not exceed 14 % per hectare for plants

of 5–10 m in height. These quantitative estimates provide new input for and constraints on models of disturbance, demography and ecosystem processes in tropical forests of widely varying structure and composition.

Tropical elevation studies have traditionally relied upon field plots that are most often, and necessarily, distributed in sparse patterns on high variable terrain. Interpretation of results from these plots is, of course, central to building our understanding of the abiotic and biotic controls over ecosystem processes such as productivity, mortality, and biogeochemical fluxes. Yet field-based measurements of canopy structural and functional traits are extremely hard to acquire, resulting in surprisingly little quantitative understanding in the scientific literature. Airborne remote sensing can provide a new perspective on canopy functional and structural traits along tropical elevation gradients, allowing for interpretations that have not been achieved from the ground vantage point, such as height distributions, gap densities, and leaf cover and light interception over heterogeneous canopy environments. Here we developed the first analysis of landscape-scale canopy functional and structural traits along an Andes-to-Amazon elevation gradient. Our integrated spectral and LiDAR measurements allowed us to draw inferences on the way elevation, terrain and soils affect the three-dimensional forest habitat and its dynamics. It also provided strong evidence based on gap-frequency, canopy height, and gap density data, supporting recent field-based estimates of high and nearly constant productivity high up into the Andes. In this context, airborne imaging spectroscopy and LiDAR provided a novel assessment totally independent of ground-based data.

The Andes-to-Amazon corridor remains virtually unexplored scientifically. With thousands of valleys, extremely diverse terrain conditions, and variable soils, there exists a vast frontier still waiting to be discussed. Airborne imaging spectroscopy and LiDAR provide new tools for quantifying an array of canopy and terrain properties on a detailed, regional scale never achieved in the field or from Earth orbit. Airborne mapping also provides geospatial information to greatly improve site selection for field plots. Our

results represent a step toward to unravelling structural and functional composition of one of the most biologically diverse regions of our planet.

References

Alves, L. F., Vieira, S. A., Scaranello, M. A., Camargo, P. B., Santos, F. A. M., Joly, C. A., and Martinelli, L. A.: Forest structure and live aboveground biomass variation along an elevational gradient of tropical Atlantic moist forest (Brazil), Forest Ecol. Manag., 260, 679–691, doi:10.1016/j.foreco.2010.05.023, 2010.

Aragâo, L. E. O. C., Malhi, Y., Metcalfe, D. B., Silva-Espejo, J. E., Jiménez, E., Navarrete, D., Almeida, S., Costa, A. C. L., Salinas, N., Phillips, O. L., Anderson, L. O., Alvarez, E., Baker, T. R., Goncalvez, P. H., Huamán-Ovalle, J., Mamani-Solórzano, M., Meir, P., Monteagudo, A., Patiño, S., Peñuela, M. C., Prieto, A., Quesada, C. A., Rozas-Dávila, A., Rudas, A., Silva Jr., J. A., and Vásquez, R.: Above- and below-ground net primary productivity across ten Amazonian forests on contrasting soils, Biogeosciences, 6, 2759–2778, doi:10.5194/bg-6-2759-2009, 2009.

Asner, G. P.: Hyperspectral remote sensing of canopy chemistry, physiology and diversity in tropical rainforests, in: Hyperspectral remote sensing of tropical and subtropical forests, edited by: Kalacska, M. and Sanchez-Azofeifa, G. A., Taylor and Francis Group, Boca Raton, Fl, 261–296, 2008.

Asner, G. P. and Heidebrecht, K. B.: Spectral unmixing of vegetation, soil and dry carbon cover in arid regions: comparing multispectral and hyperspectral observations, Int. J. Remote Sens., 23, 3939–3958, 2002.

Asner, G. P., Wessman, C. A., and Archer, S.: Scale dependence of absorption of photosynthetically active radiation in terrestrial ecosystems, Ecol. Appl., 8, 1003–1021, 1998.

Asner, G. P., Elmore, A. J., Hughes, F. R., Warner, A. S., and Vitousek , P. M.: Ecosystem structure along bioclimatic gradients in Hawai'i from imaging spectroscopy, Remote Sens. Environ., 96, 497–508, 2005.

Asner, G. P., Knapp, D. E., Kennedy-Bowdoin, T., Jones, M. O., Martin, R. E., Boardman, J., and Field, C. B.: Carnegie Airborne Observatory: In-flight fusion of hyperspectral imaging and waveform light detection and ranging (LiDAR) for three-dimensional studies of ecosystems, J. Appl. Remote Sens., 1, 013536, doi:10.1117/1.2794018, 2007.

Asner, G. P., Hughes, R. F., Vitousek, P. M., Knapp, D. E., Kennedy-Bowdoin, T., Boardman, J., Martin, R. E., Eastwood, M., and Green, R. O.: Invasive plants transform the 3-D structure of rainforests, P. Natl. Acad. Sci., 105, 4519–4523, 2008.

Asner, G. P., Clark, J. K., Mascaro, J., Galindo García, G. A., Chadwick, K. D., Navarrete Encinales, D. A., Paez-Acosta, G., Cabrera Montenegro, E., Kennedy-Bowdoin, T., Duque, Á., Balaji, A., von Hildebrand, P., Maatoug, L., Phillips Bernal, J. F., Yepes Quintero, A. P., Knapp, D. E., García Dávila, M. C., Jacobson, J., and Ordóñez, M. F.: High-resolution mapping of forest carbon stocks in the Colombian Amazon, Biogeosciences, 9, 2683–2696, doi:10.5194/bg-9-2683-2012, 2012a.

Asner, G. P., Knapp, D. E., Boardman, J., Green, R. O., Kennedy-Bowdoin, T., Eastwood, M., Martin, R. E., Anderson, C., and Field, C. B.: Carnegie Airborne Observatory-2: Increasing science data dimensionality via high-fidelity multi-sensor fusion, Remote Sens. Environ., 124, 454–465, doi:10.1016/j.rse.2012.06.012, 2012b.

Asner, G. P., Mascaro, J., Muller-Landau, H. C., Vieilledent, G., Vaudry, R., Rasamoelina, M., Hall, J. S., and van Breugel, M.: A universal airborne LiDAR approach for tropical forest carbon mapping, Oecologia, 168, 1147–1160, doi:10.1007/s00442-011-2165-z, 2012c.

Asner, G. P., Kellner, J. R., Kennedy-Bowdoin, T., Knapp, D. E., Anderson, C., and Martin, R. E.: Forest canopy gap distributions in the southern Peruvian Amazon, PLoS ONE, 8, e60875, doi:10.1371/journal.pone.0060875, 2013a.

Asner, G. P., Martin, R. E., Tupayachi, R., Anderson, C., Sinca, F., Carranza, L., and Martinez, P.: Forest canopy chemical assembly on an Amazon elevation gradient, in review, 2013b.

Baker, T. R., Phillips, O. L., Malhi, Y., Almeida, S. A. S., Arroyo, L., Di Fiore, A., Erwin, T., Killeen, T. J., Laurance, S. G., Laurance, W. F., Lewis, S. L., Lloyd, J., Manteagudo, A., Neill, D. A., Patino, S., Pitman, N. C. A., Natalino, J., Silva, M., and Martinez, R. V.: Variation in wood density determines spatial patterns in Amazonia forest biomass, Glob. Change Biol., 10, 545–562, 2004.

Landscape-scale changes in forest structure

G. P. Asner et al.

Title Page

Abstract | Introduction

Conclusions | References

Tables | Figures

◄◄ | ►►

◄ | ►

Back | Close

Full Screen / Esc

Printer-friendly Version

Interactive Discussion

Brokaw, N. V.: The definition of treefall gap and its effect on measures of forest dynamics, Biotropica, 14, 158–160, 1982.

Brokaw, N. V.: Gap-phase regeneration in a tropical forest, Ecology, 66, 682–687, 1985a.

Brokaw, N. V. L.: Treefalls, regrowth, and community structure in tropical forests, in: The ecology of natural disturbance and patch dynamics, edited by: Pickett, S. T. A., and White, P. S., Academic Press, New York, 53–69, 1985b.

Carvalho, A. L. d., Nelson, B. W., Bianchini, M. C., Plagnol, D., Kuplich, T. M., and Daly, D. C.: Bamboo-Dominated Forests of the Southwest Amazon: Detection, Spatial Extent, Life Cycle Length and Flowering Waves, PLoS ONE, 8, e54852, doi:10.1371/journal.pone.0054852, 2013.

Chambers, J. Q., Negron-Juarez, R. I., Marra, D. M., Di Vittorio, A., Tews, J., Roberts, D., Ribeiro, G. H. P. M., Trumbore, S. E., and Higuchi, N.: The steady-state mosaic of disturbance and succession across an old-growth Central Amazon forest landscape, P. Natl. Acad. Sci., 416–423, 2013.

Chazdon, R. L.: Sunflecks and their importance to forest understorey plants, Adv. Ecol. Res., 18, 1–63, 1988.

Clauset, A., Shalizi, C. R., and Newman, M. E. J.: Power-law distributions in empirical data, SIAM Review, 51, 661–703, 2009.

Denslow, J. S.: Tropical rainforest gaps and tree species diversity, Annu. Rev. Ecol. Syst., 18, 431–451, 1987.

Drake, J. B., Dubayah, R. O., Clark, D. B., Knox, R. G., Blair, J. B., Hofton, M. A., Chazdon, R. L., Weishampel, J. F., and Prince, S. D.: Estimation of tropical forest structural characteristics using large-footprint lidar, Remote Sens. Environ., 79, 305–319, 2002.

Fine, P. V. A., Mesones, I., and Coley, P. D.: Herbivores promote habitat specialization by trees in Amazonian forests, Science, 305, 663–665, doi:10.1126/science.1098982, 2004.

Fisher, J. I., Hurtt, G. C., Thomas, R. Q., and Chambers, J. Q.: Clustered disturbances lead to bias in large-scale estimates based on forest sample plots, Ecol. Lett., 11, 554–563, 2008.

Fyllas, N. M., Patiño, S., Baker, T. R., Bielefeld Nardoto, G., Martinelli, L. A., Quesada, C. A., Paiva, R., Schwarz, M., Horna, V., Mercado, L. M., Santos, A., Arroyo, L., Jiménez, E. M., Luizão, F. J., Neill, D. A., Silva, N., Prieto, A., Rudas, A., Silviera, M., Vieira, I. C. G., Lopez-Gonzalez, G., Malhi, Y., Phillips, O. L., and Lloyd, J.: Basin-wide variations in foliar properties of Amazonian forest: phylogeny, soils and climate, Biogeosciences, 6, 2677–2708, doi:10.5194/bg-6-2677-2009, 2009.

Landscape-scale changes in forest structure

G. P. Asner et al.

Title Page

Abstract | Introduction

Conclusions | References

Tables | Figures

|◄ | ►|

◄ | ►

Back | Close

Full Screen / Esc

Printer-friendly Version

Interactive Discussion

Gamon, J. A., Field, C. B., Goulden, M. L., Griffin, K. L., Hartley, A. E., Joel, G., Peñuelas, J., and Valentini, R.: Relationships between NDVI, canopy structure, and photosynthesis in three Californian vegetation types, Ecol. Appl., 5, 28–41, 1995.

Gentry, A. H.: Changes in Plant Community Diversity and Floristic Composition on Environmental and Geographical Gradients, Ann. Mo. Bot. Gard., 75, 1–34, 1988.

Girardin, C. A. J., Malhi, Y., AragÃO, L. E. O. C., Mamani, M., Huaraca Huasco, W., Durand, L., Feeley, K. J., Rapp, J., Silva-Espejo, J. E., Silman, M., Salinas, N., and Whittaker, R. J.: Net primary productivity allocation and cycling of carbon along a tropical forest elevational transect in the Peruvian Andes, Glob. Change Biol., 16, 3176–3192, doi:10.1111/j.1365-2486.2010.02235.x, 2010.

Girardin, C. A. J., Farfan-Rios, W., Garcia, K., Feeley, K. J., Jorgensen, P. M., Murakami, A. A., Pérez, L. C., Seide, R., Paniagua, N., Claros, A. F., Maldonado, C., Silman, M., Salinas, N., Reynel, C., Neill, D. A., Serrano, M., Caballero, C. J., Cuadros, M. A. T., Macía, M. J., Killeen, T. J., and Malhi, Y.: Comparison of biomass and structure in various elevation gradients in the Andes, Plant Ecology and Diversity, 6, 100–110, 2013.

Gloor, M., Phillips, O. L., Lloyd, J. J., Lewis, S. L., Malhi, Y., Baker, T. R., Lopez-Gonzalez, G., Peacock, J., Almeida, S., de Oliveira, A. C. A., Alvarez, E., Amaral, I., Arroyo, L., Aymard, G., Banki, O., Blanc, L., Bonal, D., Brando, P., Chao, K. J., Chave, J., Davila, N., Erwin, T., Silva, J., Di Fiore, A., Feldpausch, T. R., Freitas, A., Herrera, R., Higuchi, N., Honorio, E., Jimenez, E., Killeen, T., Laurance, W., Mendoza, C., Monteagudo, A., Andrade, A., Neill, D., Nepstad, D., Vargas, P. N., Penuela, M. C., Cruz, A. P., Prieto, A., Pitman, N., Quesada, C., Salomao, R., Silveira, M., Schwarz, M., Stropp, J., Ramirez, F., Ramirez, H., Rudas, A., ter Steege, H., Silva, N., Torres, A., Terborgh, J., Vasquez, R., and van der Heijden, G.: Does the disturbance hypothesis explain the biomass increase in basin-wide Amazon forest plot data, Glob. Change Biol., 15, 2418–2430, doi:10.1111/j.1365-2486.2009.01891.x, 2009.

Goward, S. N. and Huemmrich, K. F.: Vegetation canopy PAR absorptance and the normalized difference vegetation index: an assessment using the SAIL model, Remote Sens. Environ., 39, 119–140, 1992.

Hatfield, J. L.: Intercepted photosynthetically active radiation estimated by spectral reflectance, Remote Sens. Environ., 14, 65–75, 1984.

Higgins, M. A., Asner, G. P., Perez, E., Elespuru, N., Tuomisto, H., Ruokolainen, K., and Alonso, A.: Use of Landsat and SRTM Data to Detect Broad-Scale Biodiversity Patterns in Northwestern Amazonia, Remote Sensing, 4, 2401–2418, 2012.

Landscape-scale changes in forest structure

G. P. Asner et al.

Title Page

Abstract | Introduction

Conclusions | References

Tables | Figures

◄ | ►

◄ | ►

Back | Close

Full Screen / Esc

Printer-friendly Version

Interactive Discussion

Hodkinson, I. D.: Terrestrial insects along elevation gradients: species and community responses to altitude, Biol. Rev., 80, 489–513, doi:10.1017/S1464793105006767, 2005.

Hoorn, C., Wesselingh, F. P., ter Steege, H., Bermudez, M. A., Mora, A., Sevink, J., Sanmartín, I., Sanchez-Meseguer, A., Anderson, C. L., Figueiredo, J. P., Jaramillo, C., Riff, D., Negri, F. R., Hooghiemstra, H., Lundberg, J., Stadler, T., Särkinen, T., and Antonelli, A.: Amazonia Through Time: Andean Uplift, Climate Change, Landscape Evolution, and Biodiversity, Science, 330, 927–931, doi:10.1126/science.1194585, 2010.

Huasco, W. H., Girardin, C. C. A. J., Doughty, C. E., Metcalfe, D. B., Baca, L. D., Silva-Espejo, J. E., Cabrera, D. G., Aragao, L. E. O. C., Davila, A. R., Marthews, T. R., Huaraca-Quispe, L. P., Alzamora-Taype, I., Mora, L. E., Farfán-Rios, W., Cabrera, K. G., Halladay, K., Salinas-Revilla, N., Silman, M. R., Meir, P., and Malhi, Y.: Seasonal production, allocation and cycling of carbon in two mid-elevation tropical montane forest plots in the Peruvian Andes, Plant Ecol. & Divers., 1–18, doi:10.1080/17550874.2013.819042, 2013.

INGEMMET: Mapa Geologico del Peru, Instituto Geologico Minero y Metalurgico, Lima, 2000.

Kokaly, R. F., Asner, G. P., Ollinger, S. V., Martin, M. E., and Wessman, C. A.: Characterizing canopy biochemistry from imaging spectroscopy and its application to ecosystem studies, Remote Sens. Environ., 113, Supplement 1, S78–S91, doi:10.1016/j.rse.2008.10.018, 2009.

Lawton, R. O.: Canopy gaps and light penetration into a wind-exposed tropical lower montane rain forest, Can. J. Forest Res., 20, 659–667, 1990.

Lefsky, M. A., Cohen, W. B., Parker, G. G., and Harding, D. J.: Lidar remote sensing for ecosystem studies, BioScience, 52, 19–30, 2002.

Lieberman, D., Lieberman, M., Peralta, R., and Hartshorn, G. S.: Tropical forest structure and composition on a large-scale altitudinal gradient in Costa Rica, J. Ecol., 84, 137–152, 1996.

Malhi, Y., Silman, M., Salinas, N., Bush, M., Meir, P., and Saatchi, S.: Introduction: Elevation gradients in the tropics: laboratories for ecosystem ecology and global change research, Glob. Change Biol., 16, 3171–3175, doi:10.1111/j.1365-2486.2010.02323.x, 2010.

Myneni, R. B., Ramakrishna, R. N., and Running, S. W.: Estimation of global leaf area index and absorbed PAR using radiative transfer models, IEEE T. Geosci. Remote, 35, 1380–1393, 1997.

Nemani, R. and Running, S. W.: Estimating regional surface resistance to evapotranspiration from NDVI and thermal-IR AVHRR data, J. Clim. Appl. Meteorol., 28, 276–284, 1989.

Peacock, J., Baker, T. R., Lewis, S. L., Lopez-Gonzalez, G., and Phillips, O. L.: The RAIN-FOR database: monitoring forest biomass and dynamics, J. Veg. Sci., 18, 535–542, doi:10.1111/j.1654-1103.2007.tb02568.x, 2007.

Quesada, C. A., Phillips, O. L., Schwarz, M., Czimczik, C. I., Baker, T. R., Patiño, S., Fyllas, N. M., Hodnett, M. G., Herrera, R., Almeida, S., Alvarez Dávila, E., Arneth, A., Arroyo, L., Chao, K. J., Dezzeo, N., Erwin, T., di Fiore, A., Higuchi, N., Honorio Coronado, E., Jimenez, E. M., Killeen, T., Lezama, A. T., Lloyd, G., López-González, G., Luizão, F. J., Malhi, Y., Monteagudo, A., Neill, D. A., Núñez Vargas, P., Paiva, R., Peacock, J., Peñuela, M. C., Peña Cruz, A., Pitman, N., Priante Filho, N., Prieto, A., Ramírez, H., Rudas, A., Salomão, R., Santos, A. J. B., Schmerler, J., Silva, N., Silveira, M., Vásquez, R., Vieira, I., Terborgh, J., and Lloyd, J.: Basin-wide variations in Amazon forest structure and function are mediated by both soils and climate, Biogeosciences, 9, 2203–2246, doi:10.5194/bg-9-2203-2012, 2012.

Raich, J. W., Russell, A. E., and Vitousek, P. M.: Primary productivity and ecosystem development along an elevational gradient on Mauna Loa, Hawaii, Ecology, 78, 707–722, 1997.

Regard, V., Lagnous, R., Espurt, N., Darrozes, J., Baby, P., Roddaz, M., Calderon, Y., and Hermoza, W.: Geomorphic evidence for recent uplift of the Fitzcarrald Arch (Peru): A response to the Nazca Ridge subduction, Geomorphology, 107, 107–117, http://dx.doi.org/10.1016/j.geomorph.2008.12.003, 2009.

Riano, D., Chuvieco, E., Ustin, S., Zomer, R., Dennison, P., Roberts, D., and Salas, J.: Assessment of vegetation regeneration after fire through multitemporal analysis of AVIRIS images in the Santa Monica Mountains, Remote Sens. Environ., 79, 60–71, 2002.

Roberts, D. A., Green, R. O., and Adams, J. B.: Temporal and spatial patterns in vegetation and atmospheric properties from AVIRIS, Remote Sens. Environ., 62, 223–240, 1997.

Sellers, P. J., Los, S. O., Tucker, C. J., Justice, C. O., Dazlich, D. A., Collatz, G. J., and Randall, D. A.: A global 1° by 1° NDVI data set for climate studies. Part 2: The generation of global fields of terrestrial biophysical parameters from the NDVI, Int. J. Remote Sens., 15, 3519–3545, 1995.

Silman, M. R.: Plant species diversity in Amazonian forests, in: Tropical rain forest responses to climate change, edited by: Bush, M. and Flenly, J., Springer-Praxis, London, 2006.

Tanner, E. V. J., Vitousek, P. M., and Cuevas, E.: Experimental investigation of nutrient limitation of forst growth on wet tropical mountains, Ecology, 79, 10–23, 1998.

Terborgh, J.: Maintenance of diversity in tropical forests, Biotropica, 24, 283–292, 1992.

Landscape-scale changes in forest structure

G. P. Asner et al.

Full Screen / Esc

Printer-friendly Version

Interactive Discussion

Ticehurst, C., Held, A., and Phinn, S.: Integrating JERS-1 imaging radar and elevation models for mapping tropical vegetation communities in Far North Queensland, Australia, Photogramm. Eng. Rem. S., 70, 1259–1266, 2004.

Tuomisto, H., Poulsen, A. D., Ruokolainen, K., Moran, R. C., Quintana, C., Celi, J., and Canas, G.: Linking floristic patterns with soil heterogeneity and satellite imagery in Ecuadorian Amazonia, Ecol. Appl., 13, 352–371, 2003.

Ustin, S. L., Roberts, D. A., Gamon, J. A., Asner, G. P., and Green, R. O.: Using imaging spectroscopy to study ecosystem processes and properties, Bioscience, 54, 523–534, 2004.

Vitousek, P. M., Matson, P. A., and Turner, D. R.: Elevational and age gradients in Hawaiian montane rainforest: foliar and soil nutrients, Oecologia, 77, 565–570, 1988.

Vitousek, P. M., Aplet, G., and Turner, D.: The Mauna Loa environmental matrix: foliar and soil nutrients, Oecologia, 89, 372–382, 1992.

Wessman, C. A., Nel, E. M., Bateson, C. A., and Asner, G. P.: A method to access absolute fIPAR of vegetation in spatially complex ecosystems, Proceedings of the Seventh Airborne Earth Science Workshop, NASA Jet Propulsion Laboratory, Pasadena, CA, 9, 409–418, 1998.

White, E. P., Enquist, B. J., and Green, J. L.: On estimating the exponent of power-law frequency distributions, Ecology, 89, 905–912, 2008.

Title Page

Abstract | Introduction

Conclusions | References

Tables | Figures

|◀ | ▶|

◀ | ▶

Back | Close

Full Screen / Esc

Printer-friendly Version

Interactive Discussion

Table 1. Description of 25 ha landscapes mapped and analyzed in the Andes-to-Amazon corridor. Soil orders follow the US Department of Agriculture (USDA) soil taxonomy system. Sites labeled with an asterisk (*) are those considered to be higher in soil fertility, as reported in the literature.

Site Name	Center Latitude	Center Longitude	MAP (mm)	MAT (C)	Soil Order
Sucusari; SUC-01	−3.2519	−72.9078	2754	26.2	Ultisol
Allpahuayo; ALP-01*	−3.9491	−73.4346	2760	26.3	Inceptisol
Jenaro Herrera; JEN-11	−4.8781	−73.6295	2700	26.6	Ultisol
Sucusari; SUC-05	−3.2558	−72.8942	2754	26.2	Ultisol
Jenaro Herrera; JEN-12	−4.8990	−73.6276	2700	26.6	Entisol
Allpahuayo; ALP-40	−3.9410	−73.4400	2760	26.3	Entisol
Allpahuayo; ALP-30	−3.9543	−73.4267	2760	26.3	Ultisol
Cuzco Amazonico; CUZ-03*	−12.5344	−69.0539	2600	24.7	Inceptisol
Tambopata; TAM-06*	−12.8385	−69.2960	2600	24.0	Inceptisol
Tambopata; TAM-09*	−12.8309	−69.2843	2600	24.0	Inceptisol
Tambopata; TAM-05	−12.8303	−69.2705	2600	24.0	Ultisol
Paujil; PJL-01	−10.3250	−75.2622	5020	23.1	Ultisol
Paujil; PJL-02	−10.3300	−75.2613	5020	23.1	Ultisol
San Pedro; SPD-02*	−13.0491	−71.5365	4628	18.5	Inceptisol
San Pedro; SPD-01*	−13.0475	−71.5423	4341	18.5	Inceptisol
Mirador; TRU-08*	−13.0702	−71.5559	4341	18.5	Entisol
Trocha Union; TRU-04*	−13.1055	−71.5893	2678	13.0	Inceptisol
Esperanza; ESP-01*	−13.1751	−71.5948	1705	12.5	Inceptisol
Trocha Union; TRU-03*	−13.1097	−71.5995	2678	13.0	Inceptisol
Trocha Union; TRU-01*	−13.1136	−71.6069	2448	13.0	Inceptisol

Table 2. Topographic variables for 25 ha Andes-to-Amazon landscapes measured with the CAO LiDAR. Mean values for ground elevation, slope, aspect, and canopy height are provided with standard deviations in parentheses. The canopy shape ratio is the height of peak canopy volume (P) divided by the 99th percentile total canopy height (H). The canopy gap size parameter (λ) is the negative slope of the power-law relationship between gap size and frequency.

Site	Elevation (m)	Slope (deg)	Aspect (deg)	Canopy Height* (m)	Canopy Shape** ($P:H$)	Gap Size Param*** (λ)
SUC-01	116.6 (6.2)	9.7 (5.2)	187.9 (106.8)	24.5 (7.3)	0.558	1.84
ALP-01	131.0 (5.7)	8.1 (6.9)	176.4 (107.8)	22.5 (6.8)	0.629	1.96
JEN-11	131.2 (2.4)	9.4 (7.3)	192.9 (102.7)	23.7 (6.3)	0.600	1.93
SUC-05	131.8 (4.9)	2.1 (1.3)	173.8 (101.9)	24.9 (6.9)	0.595	1.81
JEN-12	134.9 (0.6)	4.6 (2.9)	175.3 (109.8)	16.5 (6.5)	0.417	2.03
ALP-40	141.5 (1.3)	5.0 (3.7)	153.8 (95.0)	15.1 (6.5)	0.290	2.21
ALP-30	142.4 (6.7)	2.4 (2.2)	179.1 (102.6)	21.9 (7.0)	0.564	1.84
CUZ-03	204.9 (1.2)	3.0 (2.2)	177.7 (105.0)	24.0 (9.9)	0.609	1.88
TAM-06	214.8 (4.3)	4.0 (5.7)	169.4 (109.1)	18.2 (9.5)	0.500	1.78
TAM-09	219.2 (1.8)	4.4 (4.1)	192.9 (100.8)	21.1 (7.7)	0.548	1.80
TAM-05	223.3 (2.4)	6.9 (8.4)	186.2 (104.9)	21.0 (6.2)	0.526	1.91
PJL-01	496.2 (5.6)	6.7 (5.6)	182.3 (111.3)	21.2 (6.1)	0.568	1.87
PJL-02	884.1 (64.8)	31.8 (9.6)	121.4 (110.8)	20.8 (7.7)	0.512	1.85
SPD-02	1493.9 (58.6)	39.0 (10.1)	143.5 (80.8)	18.4 (8.4)	0.442	1.77
SPD-01	1712.9 (58.8)	40.1 (9.8)	141.9 (92.3)	16.9 (8.0)	0.462	1.88
TRU-08	1831.5 (83.0)	41.8 (10.7)	137.0 (111.2)	12.1 (6.0)	0.200	1.74
TRU-04	2719.1 (56.5)	28.6 (12.0)	189.8 (119.9)	14.1 (6.7)	0.091	1.73
ESP-01	2868.3 (73.3)	29.5 (10.2)	246.4 (122.9)	9.0 (6.0)	0.115	1.79
TRU-03	2989.5 (67.1)	37.6 (11.8)	129.3 (100.1)	12.9 (6.4)	0.125	1.79
TRU-01	3379.3 (67.0)	34.3 (11.1)	144.3 (120.8)	8.9 (5.6)	0.077	1.86

Table 3. Inter-relationships of landscape-scale canopy functional and structural traits along the elevation gradient. Values are Pearson Product Moment correlation coefficients (r) with bold font indicating p values ≤ 0.05.

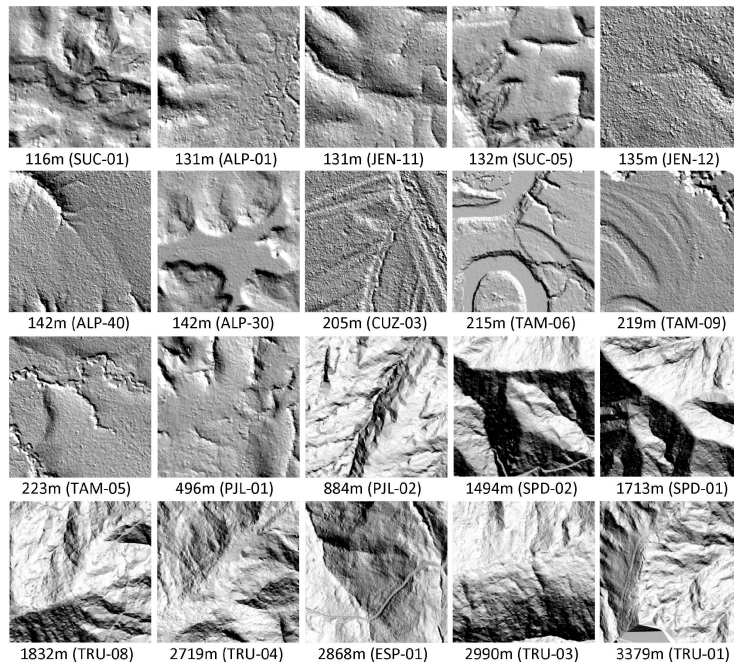| | NDVI | PV | NPV | S | fIPAR | Height | $P:H$ | Gap-size λ | Number of gaps in a size class (m^2) per ha | | | | | | | % cover in height class (m) | | |
									≤ 5	5–10	10–20	20–50	50–100	100–200	≥ 200	1–3	3–5	5–10
NDVI	–	0.42	**−0.58**	**−0.63**	−0.66	**0.83**	**0.86**	0.18	**−0.77**	**−0.79**	**−0.74**	**−0.82**	**−0.58**	**−0.73**	−0.21	**−0.68**	**−0.82**	**−0.70**
PV		–	**−0.97**	**0.75**	−0.21	0.45	**0.53**	−0.42	−0.06	−0.10	−0.06	−0.09	0.04	−0.10	0.17	−0.13	−0.38	**−0.62**
NPV			–	**−0.87**	0.10	**−0.58**	**−0.66**	0.23	0.28	0.31	0.28	0.31	0.17	0.32	−0.05	0.31	**0.53**	**0.67**
S				–	0.04	**0.61**	**0.63**	0.11	**−0.55**	**−0.49**	**−0.55**	**−0.48**	**−0.52**	**−0.61**	−0.29	**−0.52**	**−0.59**	**−0.57**
fIPAR					–	0.35	0.38	0.16	**−0.64**	**−0.50**	**−0.55**	**−0.54**	**−0.50**	**−0.47**	**−0.47**	**−0.55**	**−0.55**	**−0.48**
Height						–	**0.94**	0.04	**−0.82**	**−0.82**	**−0.71**	**−0.75**	**−0.68**	**−0.63**	−0.35	**−0.71**	**−0.87**	**−0.94**
$P:H$							–	0.13	**−0.76**	**−0.85**	**−0.71**	**−0.79**	**−0.65**	**−0.65**	−0.17	**−0.66**	**−0.86**	**−0.90**
Gap-size λ								–	**−0.41**	**−0.52**	**−0.60**	**−0.55**	**−0.53**	**−0.53**	−0.26	**−0.48**	−0.25	0.16
Gap ≤ 5 m^2									–	**0.92**	**0.89**	**0.87**	**0.90**	**0.87**	**0.68**	**0.89**	**0.81**	**0.63**
Gap 5–10 m^2										–	**0.90**	**0.96**	**0.80**	**0.80**	0.37	**0.86**	**0.87**	**0.67**
Gap 10–20 m^2											–	**0.92**	**0.86**	**0.86**	0.55	**0.94**	**0.86**	**0.56**
Gap 20–50 m^2												–	**0.75**	**0.86**	0.37	**0.90**	**0.90**	**0.62**
Gap 50–100 m^2													–	**0.87**	**0.76**	**0.82**	**0.69**	0.48
Gap 100–200 m^2														–	**0.62**	**0.85**	**0.75**	0.46
Gap ≥ 200 m^2															–	**0.64**	0.38	0.18
1–3 m Cover																–	**0.90**	0.58
3–5 m Cover																	–	**0.85**
5–10 m Cover																		–

Fig. 1. Shaded relief maps showing the terrain underlying forests along an Andes-to-Amazon elevation gradient of 116 m to 3379 m a.s.l. Sites names are provided in parentheses, matching those listed in Table 1. These maps are 1.1 m spatial resolution.

116m (SUC-01) 131m (ALP-01) 131m (JEN-11) 132m (SUC-05) 135m (JEN-12)

142m (ALP-40) 142m (ALP-30) 205m (CUZ-03) 215m (TAM-06) 219m (TAM-09)

223m (TAM-05) 496m (PJL-01) 884m (PJL-02) 1494m (SPD-02) 1713m (SPD-01)

1832m (TRU-08) 2719m (TRU-04) 2868m (ESP-01) 2990m (TRU-03) 3379m (TRU-01)

116m (SUC-01)   131m (ALP-01)   131m (JEN-11)   132m (SUC-05)   135m (JEN-12)

142m (ALP-40)   142m (ALP-30)   205m (CUZ-03)   215m (TAM-06)   219m (TAM-09)

223m (TAM-05)   496m (PJL-01)   884m (PJL-02)   1494m (SPD-02)   1713m (SPD-01)

1832m (TRU-08)   2719m (TRU-04)   2868m (ESP-01)   2990m (TRU-03)   3379m (TRU-01)
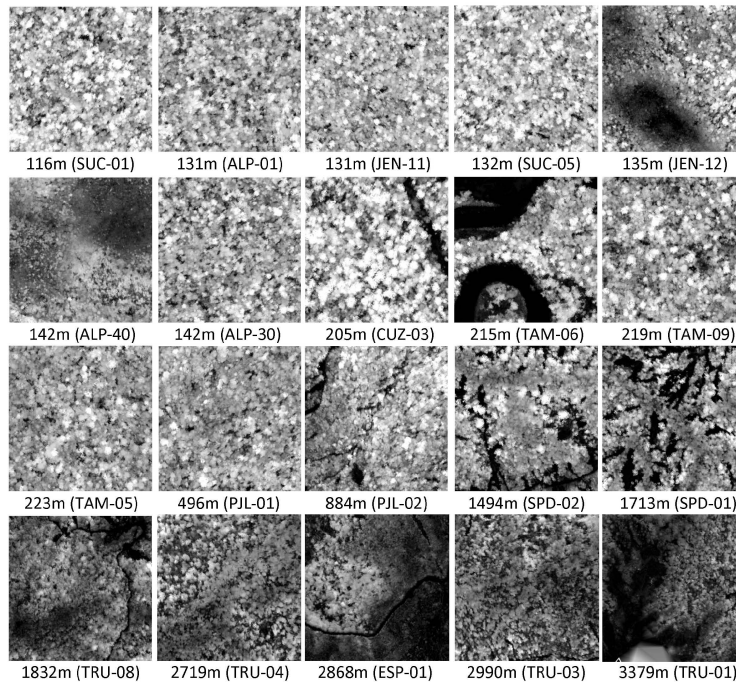
Fig. 2. Vegetation canopy height after removing variation in terrain (see Fig. 1) at 1.1 m spatial resolution throughout forests along the elevation gradient. Sites names are provided in parentheses, matching those listed in Table 1.
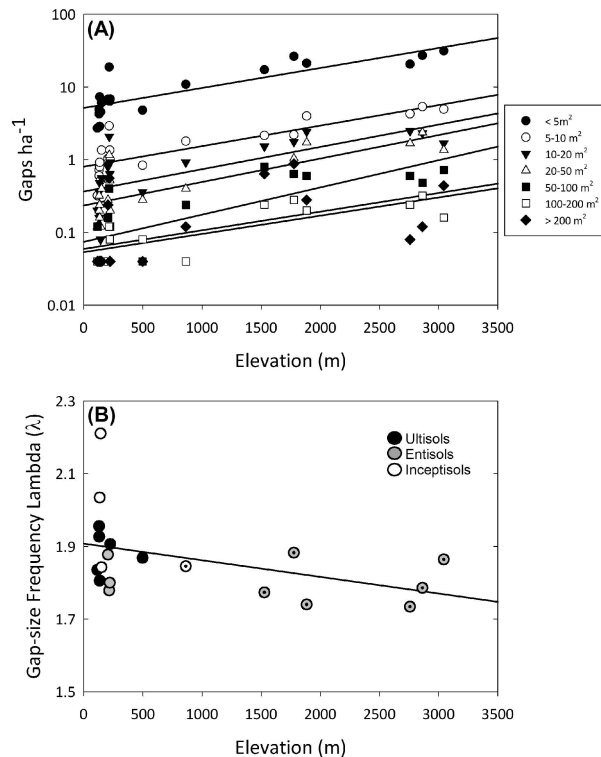
Fig. 3. (A) Changes in mean canopy gap density with increasing elevation for each 25 ha forest landscape. Gaps are computed to 2 m above ground level (Brokaw, 1985a) in seven gap-size classes from $< 5\,\text{m}^2$ to $> 200\,\text{m}^2$ per gap. **(B)** Changes in the gap-size frequency scaling coefficient λ for each landscape along the elevation gradient. Symbols are colored by USDA soil order; and dots within circle indicate sites included in elevation-based regression of main text.
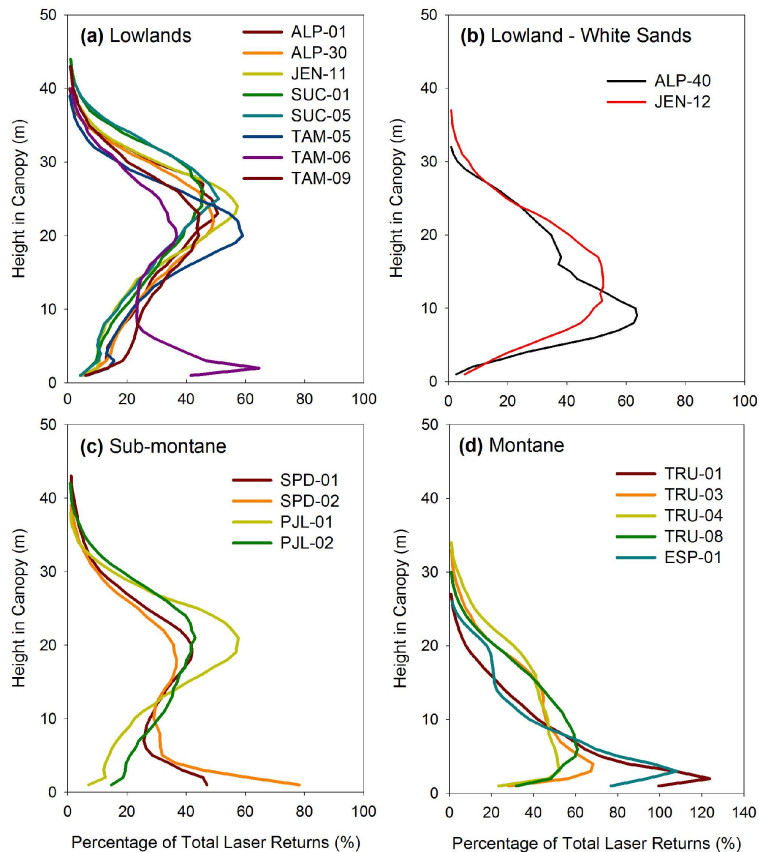
Fig. 4. Mean canopy vertical profile for **(a)** lowland, **(b)** lowland on white sand soils, **(c)** sub-montane, and **(d)** montane forest landscapes. Site names match those provided in Table 1.

Fig. 5. Images showing understory plant cover (presence vs. absence) in 1–3 m (red), 3–5 m (green), and 5–10 m (blue) height classes. Images are arranged by elevation to match Figs. 1 and 2. Site names match those listed in Table 1.

Title Page

Abstract   Introduction

Conclusions   References

Tables   Figures

◄   ►►

◄   ►

Back   Close

Full Screen / Esc

Printer-friendly Version

Interactive Discussion
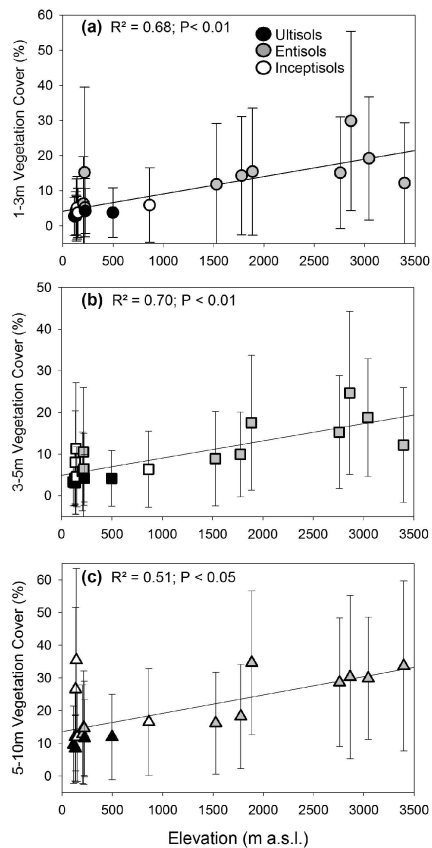
Fig. 6. Changes in mean understory canopy cover along the elevation gradient at **(a)** 1–3 m, **(b)** 3–5 m, and **(c)** 5–10 m height classes from Fig 5. Error bars indicate standard deviation of canopy cover in each 25 ha forest landscape. Symbols are colored by USDA soil order.
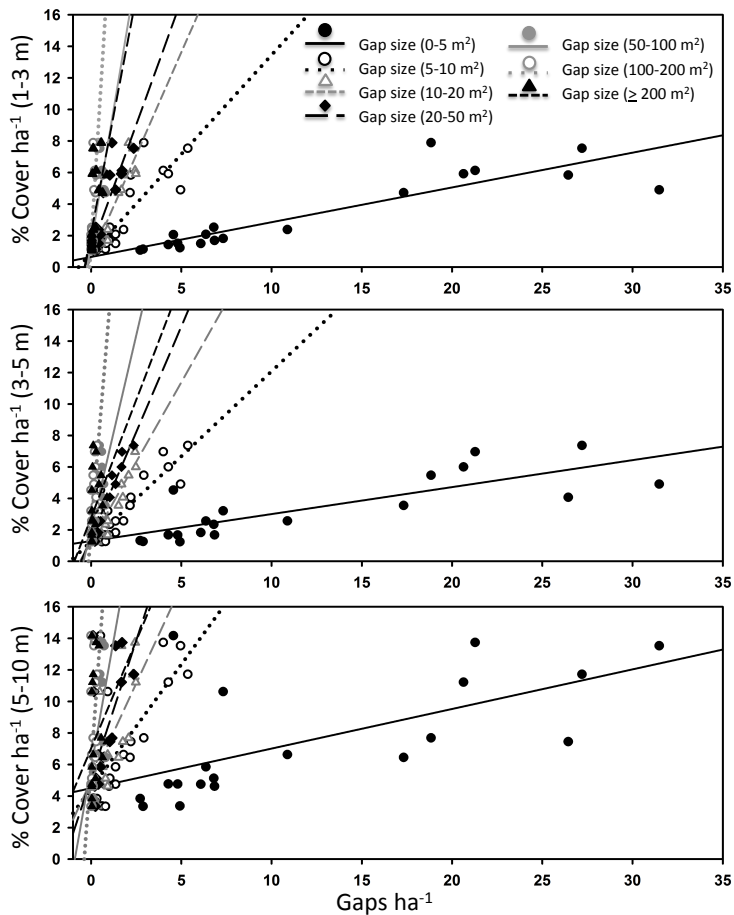
Fig. 7. Relationships between mean canopy gap density (see Fig. 3a) and percentage under-story canopy cover (see Fig. 6) in seven gap-size classes from $< 5\,\mathrm{m}^2$ to $> 200\,\mathrm{m}^2$ per gap.

116m (SUC-01) 131m (ALP-01) 131m (JEN-11) 132m (SUC-05) 135m (JEN-12)

142m (ALP-40) 142m (ALP-30) 205m (CUZ-03) 215m (TAM-06) 219m (TAM-09)

223m (TAM-05) 496m (PJL-01) 884m (PJL-02) 1494m (SPD-01) 1713m (SPD-02)

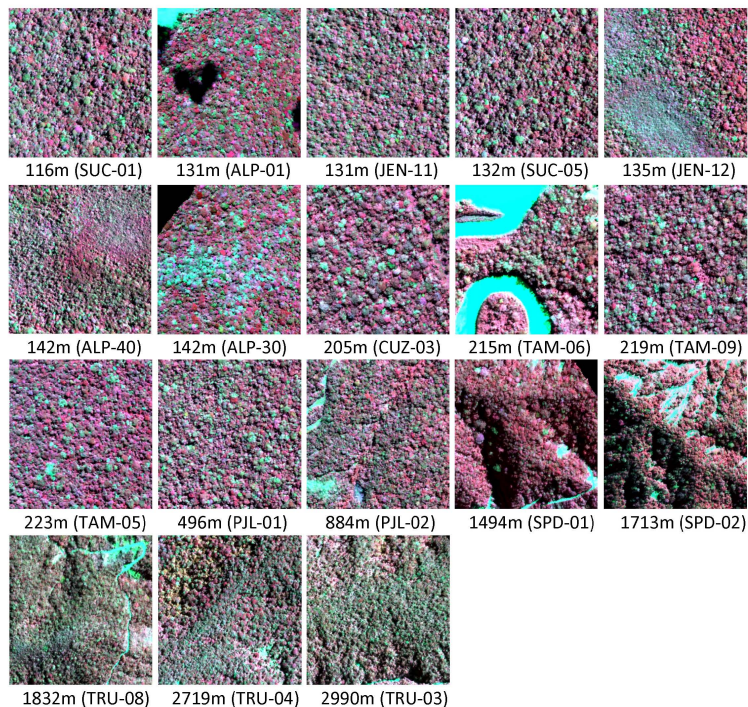1832m (TRU-08) 2719m (TRU-04) 2990m (TRU-03)

Fig. 8. Changes in narrowband, near-infrared reflectance spectroscopy of forests along the elevation gradient. Images are a combination of near-infrared (800–809 nm), red (650–659 nm), and green (550–559 nm) reflectance. Black areas are image edges, cloud shadows (ALP-01), and/or topographic shade (SPD-01/02).

Title Page

Abstract | Introduction

Conclusions | References

Tables | Figures

|◀ | ▶|

◀ | ▶

Back | Close

Full Screen / Esc

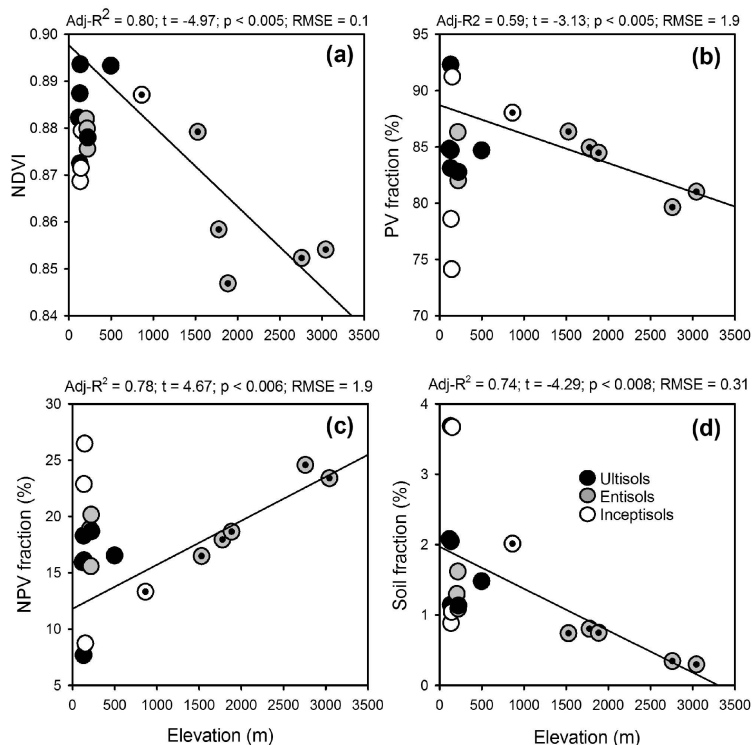Printer-friendly Version

Interactive Discussion

Fig. 9. Elevation-based changes in **(a)** NDVI, **(b)** PV fraction, **(c)** NPV fraction, and **(a)** soil fraction derived from imaging spectroscopy. Data are means for each 25 ha landscape. Symbols are colored by USDA soil order; and dots within circle indicate sites included in elevation-based regression of main text.

Discussion Paper | Discussion Paper | Discussion Paper | Discussion Paper

BGD

10, 15415–15454, 2013

Landscape-scale changes in forest structure

G. P. Asner et al.

Title Page

Abstract   Introduction

Conclusions   References

Tables   Figures

|◄   ►|

◄   ►

Back   Close

Full Screen / Esc

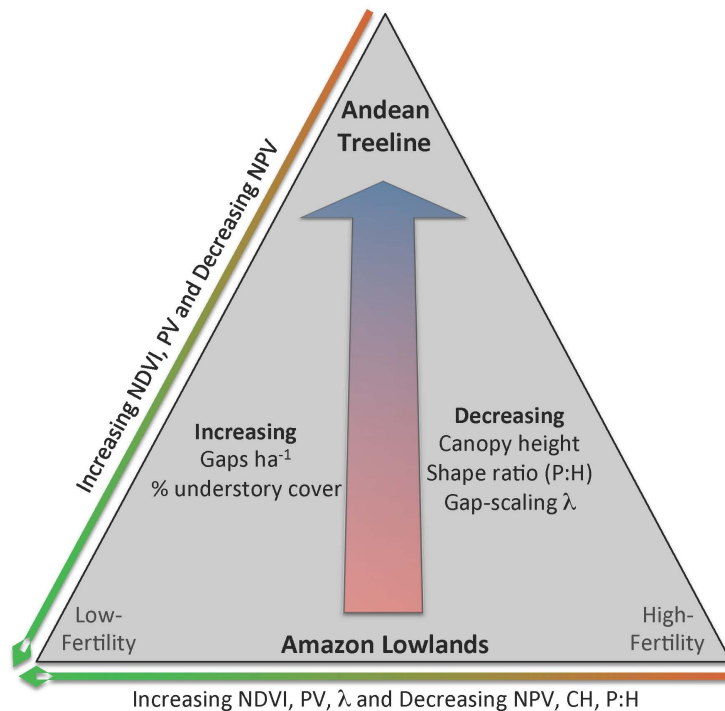Printer-friendly Version

Interactive Discussion

Fig. 10. Diagrammatic summary of all results developed throughout the study. As elevation increases from the Amazon lowlands to Andean treeline, the forest canopy undergoes increases in canopy gap density and understory plant cover, while canopy height and shape ratio ($P : H$) decrease. The gap-scaling coefficient λ decreases slightly as well. In contrast, functional trait metrics of NDVI and PV increase, while NPV decreases, from montane systems down to the low-fertility sites in the lowlands. A similar trend occurs from high to low fertility lowland sites. Additionally, canopy height and the shape ratio decrease from high to low fertility sites within the lowlands.

Title Page

Abstract | Introduction

Conclusions | References

Tables | Figures

|◄ | ►|

◄ | ►

Back | Close

Full Screen / Esc

Printer-friendly Version

Interactive Discussion

116m (SUC-01) 131m (ALP-01) 131m (JEN-11) 132m (SUC-05) 135m (JEN-12)

142m (ALP-40) 142m (ALP-30) 205m (CUZ-03) 215m (TAM-06) 219m (TAM-09)

223m (TAM-05) 496m (PJL-01) 884m (PJL-02) 1494m (SPD-01) 1713m (SPD-02)

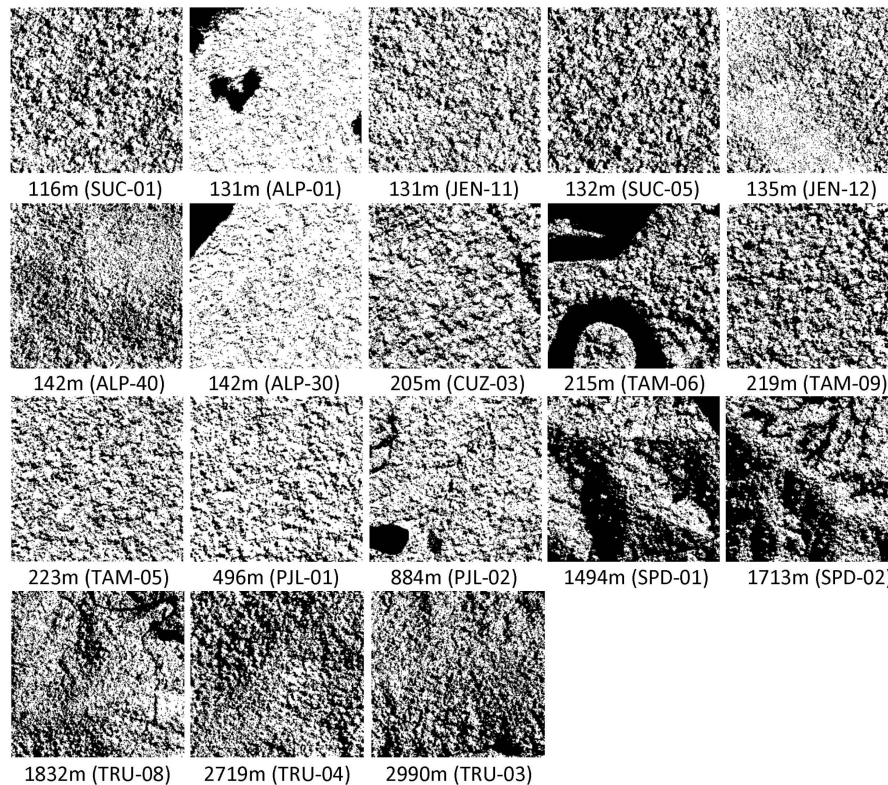1832m (TRU-08) 2719m (TRU-04) 2990m (TRU-03)

Fig. A1. Shade, ground and water mask (black areas) developed from airborne LiDAR and applied to all imaging spectrometer analyses (see Fig. 8).